



Crustal mechanics control the geometry of mountain belts. Insights from numerical modelling



Katharina Vogt*, Liviu Matenco, Sierd Cloetingh

Department of Earth Sciences, Utrecht University, Budapestlaan 6, 3584 CD Utrecht, Netherlands

ARTICLE INFO

Article history:

Received 6 June 2016

Received in revised form 28 October 2016

Accepted 8 November 2016

Available online 19 December 2016

Editor: A. Yin

Keywords:

collision
mountain belt
continental subduction
double vergent orogen
numerical modelling

ABSTRACT

Continental collision forms mountain ranges that have shaped much of Earth's topography. Yet, the process by which material is transported and redistributed in collision zones remains debatable. Here we present a series of two-dimensional thermo-mechanical experiments on continent–continent collision zones to investigate the role of crustal strength in terms of geometry, deformation and exhumation. Depending on the crustal rheology, rate of collision and initial temperature distribution, continental collision may form double vergent orogens or result in continental subduction. Double vergent orogens are characterized by subduction of the lithospheric mantle, diffuse fore- and highly localized retro-shears, elevated topographies, and exhumation of high grade metamorphic rocks. In contrast, continental subduction results in subduction of lower continental crust, the formation of a wedge shaped Moho, a foreland propagating deformation zone, “lower” topographic build-up and exhumation of low grade metamorphic rocks. It is the combination of strength variations and ambient conditions that determines the geometry of mountain belts. Strong rheological coupling of upper and lower crust forms double vergent orogens; low rheological coupling of upper and lower crust results in continental subduction.

© 2016 Published by Elsevier B.V.

1. Introduction

When continents collide mountain ranges with high topographies and complex (internal) geometries are formed. Tectonically induced stresses result in intense deformation with crustal thrusting being the primary response. Hence, crustal material is transported and redistributed within an orogen, destroying its original rock sequence. Constraints on the final crustal architecture come from surface geology, deep seismic reflection profiles and teleseismic tomography, but the mechanism that lead to its final structure remain debatable.

Early analytical (Davis et al., 1983), analogue (Malavieille, 1984) and numerical studies (Willett et al., 1993; Beaumont et al., 1996) of orogeny have focused solely on the frictional (plastic) behaviour of the continental crust, by applying a local velocity condition at its base. The resulting crustal structure is highly asymmetric with strain being more diffuse in the foreland and highly localized in the hinterland. Typical examples to which these models have successfully been applied include the Swiss Alps, the New Zealand Alps and the Pyrenees (e.g.: Beaumont et al., 1996; Jammes and

Huismans, 2012; Erdős et al., 2014). The deformation pattern in such type of experiments is strongly conditioned by the velocity discontinuity at the base of the crust that excludes any involvement of mantle lithosphere. Several studies have subsequently explored the impact of thermally activated viscous creep and plastic yielding using a similar setup (Beaumont and Quinlan, 1994; Willett, 1999; Pfiffner et al., 2000; Ellis et al., 2001), but the geometry of the resulting orogen is comparable to previous models using similar boundary conditions.

More recent analogue modelling studies have challenged this idea by demonstrating that deformation might be restricted to the lower plate and lack any retro-wedge formation (Willingshofer et al., 2013). Similar results were obtained from numerical simulations performed on a lithospheric scale that have stressed the importance of rheological stratification on the relationship between subduction of continental lithosphere, strain distribution and the resulting geometry of the collisional orogen (Jammes and Huismans, 2012; Erdős et al., 2014). Common examples of orogens, where no significant upper plate deformation has been observed include the Carpathians (Matenco et al., 2010), the Apennines (Carminati and Doglioni, 2012), parts of the Greater Caucasus (Forte et al., 2014), and the South East Asia collisional zones (Morley, 2012).

* Corresponding author.

E-mail address: k.j.vogt@uu.nl (K. Vogt).

Table 1

Material properties. ρ = initial density. Wet qtz = wet quartzite, plag = plagioclase (anorthite 75%), dry ol = dry olivine, wet ol = wet olivine after Ranalli (1995) and references therein. A_D is the pre-exponential factor, n is the stress exponent, E_a is the activation energy, V_a is the activation volume, ϕ is the friction angle, and C is the cohesion. Strain weakening is applied within a strain interval of 0–1 at which the friction angle ($\sin(\phi)$) and cohesion (C) are decreased. H_r = radioactive heat production, C_p = isobaric heat capacity, α = coefficient of thermal expansion, β = coefficient of thermal compressibility, k = thermal conductivity, $A = T[K] + 77$, $B = 0.00004 \times P$ [MPa].

Material properties:	Sediment	Upper crust decoupled	Upper crust coupled	Lower crust	Mantle	Weak shear zone
ρ [kg/m ³]	2600	2700	2700	2900	3300	3200
Flow law	wet qtz	wet qtz	plag	plag	dry ol	wet ol
$1/A_D$ [Pa ⁿ s]	1.97×10^{17}	1.97×10^{17}	4.80×10^{22}	4.80×10^{22}	3.98×10^{16}	5.01×10^{20}
n	2.3	2.3	3.2	3.2	3.5	4.0
E_a [J]	154×10^3	154×10^3	238×10^3	238×10^3	532×10^3	470×10^3
V_a [J/bar]	0.8	0.8	0.8	0.8	0.8	0.8
$\sin(\phi)$	0.20–0.10	0.30–0.15	0.30–0.15	0.30–0.15	0.60–0.30	0.10–0.05
c [Pa]	1×10^{-6}	1×10^{-6}	1×10^{-6}	1×10^{-6}	1×10^{-6}	1×10^{-6}
H_r [μ W/m ³]	2.0	1.8	1.8	0.18	0.022	0.022
C_p [J/kg K]	1000	1000	1000	1000	1000	1000
α [1/K]	3×10^{-5}	3×10^{-5}	3×10^{-5}	3×10^{-5}	3×10^{-5}	3×10^{-5}
β [1/MPa]	1×10^{-5}	1×10^{-5}	1×10^{-5}	1×10^{-5}	1×10^{-5}	1×10^{-5}
k [W/m/K]	$[0.64 + 807/A]$ $\times \exp(B)$	$[0.64 + 807/A]$ $\times \exp(B)$	$[0.64 + 807/A]$ $\times \exp(B)$	$[1.18 + 474/A]$ $\times \exp(1 + B)$	$[0.73 + 1293/A]$ $\times \exp(1 + B)$	$[0.73 + 1293/A]$ $\times \exp(1 + B)$

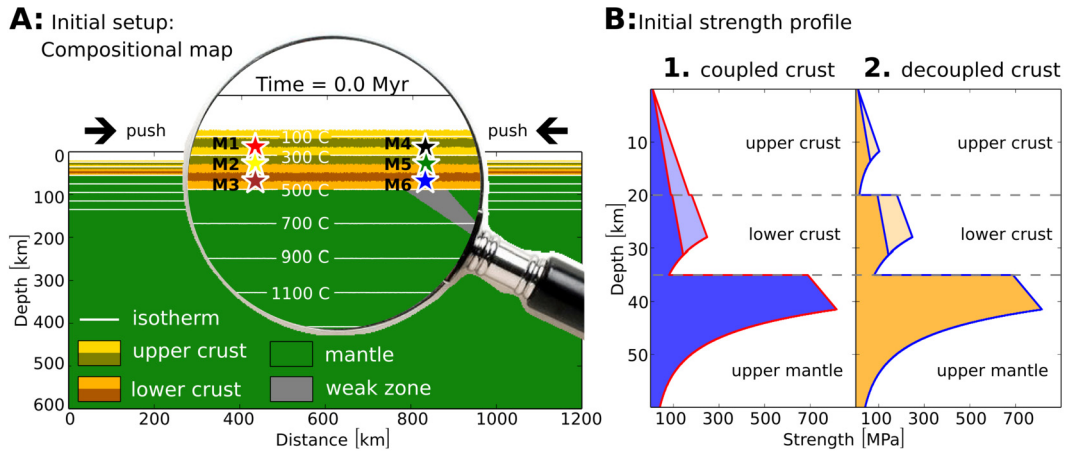


Fig. 1. A: Cross-section of the initial setup. M1–M6 (stars) denote markers (rocks) that have been traced through space and time to compute pressure–temperature paths. **B:** Initial strength profile of the continental lithosphere for a constant strain rate of $\dot{\epsilon} = 10^{-14} \text{ s}^{-1}$. Two initial strength profiles are used: coupled and decoupled crust (left and right, respectively). Strain weakening is applied within a strain interval of 0–1, which results in lower plastic strength. The light blue and yellow colours mark the initial crustal strength of the model. The dark blue and yellow colour mark the crustal strength of the model after strain weakening. See Table 1 for all material properties. (For interpretation of the references to colour in this figure, the reader is referred to the web version of this article.)

In this study we use numerical high-resolution thermo-mechanical models to investigate the impact of crustal rheology upon continental collision. We show that the strength distribution within the continental crust imposes major implications on the mode of deformation, the final crustal architecture and the exhumation pattern.

2. Methods

All numerical experiments were performed with the I2VIS code (Gerya and Yuen, 2003). This code is based on conservative finite differences and a marker-in-cell technique. The momentum, continuity and energy equations are solved on an Eulerian frame. Physical properties are transported by Lagrangian markers that move according to the velocity field interpolated from the fix grid. The model uses non-Newtonian visco-plastic rheologies to simulate multiphase flow (Table 1) and is designed to study the dynamic processes during continental collision.

2.1. Model setup

The computational domain is two-dimensional and covers 1200 km \times 600 km with a resolution of 1391 \times 451 nodal points (Fig. 1). The spacing of the gridlines increases from 10 \times 4 km

to 0.5 \times 0.5 km toward the centre of the domain, where highest deformation occurs, i.e. area of orogeny (500 km \times 100 km) (Gerya, 2010b). The left, right and upper boundary of the model are free slip. The lower boundary is open and satisfies an external free slip boundary condition below the box at 996 km depth (Gerya, 2010b).

The continental crust is homogeneous and has a total thickness of 35 km. It is subdivided into 20 km of felsic and 15 km of mafic rocks. The underlying mantle is composed of dry olivine. An internally prescribed velocity field within the convergence condition region ensures horizontal compression between two continental blocks, representing collision. A weak zone with low plastic strength and wet olivine rheology at the bottom of the continental crust represents a suture zone, separating two continental domains after the closure of an ocean (Fig. 1). This suture zone provides efficient decoupling between the colliding plates and enables subduction of the incoming mantle lithosphere beneath the collisional orogen (Burg and Gerya, 2005; Willingshofer et al., 2013).

The thermal boundary conditions are 0 °C at the upper boundary and 0 heat flux across the vertical boundaries. A thermal gradient of 25 °C/km is used for the uppermost 10 km of the continental lithosphere, followed by a lower gradient of 10 °C/km until a temperature of 1330 °C at the lithosphere–asthenosphere boundary is reached. This initial gradient results in a Moho–

Table 2

Experiments described in the text. Wet qtz = wet quartzite, plag = plagioclase (anorthite 75%).

Exp. no.	Moho [°C]	LAB [km]	Rheology		Convergence rate [cm/yr]	Surface processes [mm/yr]	
			Upper crust	Lower crust		Erosion	Sedimentation
1	500	118	plag	plag	1	0.9	0.09
2	500	118	wet qtz	plag	1	0.9	0.09
3	500	118	plag	plag	0.5	0.9	0.09
4	500	118	plag	plag	5	0.9	0.09
5	500	118	wet qtz	plag	0.5	0.9	0.09
6	500	118	wet qtz	plag	5	0.9	0.09
7	625	82	wet qtz	plag	1	0.9	0.09
8	500	118	wet qtz	wet qtz	1	0.9	0.09
9	500	118	wet qtz	plag	1	no	no

temperature of 500 °C and a lithosphere–asthenosphere boundary at 118 km depth. For the asthenospheric mantle a thermal gradient of 0.5 °C/km is used. All material properties are summarized in Table 1.

To allow for topographic build up of the lithosphere a layer of a 20 km thick layer of low viscosity (10^{18} Pa s) and low density (1 kg/m^3) is implemented above the lithosphere. The large viscosity contrast between this layer and the lithosphere minimizes shear stresses ($<10^4$ Pa) making it an efficient free surface. At surface levels this material is exposed to sedimentary and erosional processes.

2.2. Rheology

The rheologies used in this study are visco-plastic. Viscous deformation is computed as a combination of dislocation and diffusion creep and depends on temperature, pressure and strain rate. A smooth transition between diffusion creep and dislocation creep is assumed to occur at 10^4 Pa (Turcotte and Schubert, 2002).

The viscosity for dislocation creep is defined as follows (Ranalli, 1995):

$$\eta_{\text{creep}} = \frac{\dot{\epsilon}_{II}^{\frac{1-n}{n}}}{A_D^{\frac{1}{n}}} \exp\left(\frac{E_a + PV_a}{nRT}\right)$$

where $\dot{\epsilon}_{II}$ is the second invariant of the strain rate tensor. A_D (pre-exponential factor), E_a (activation energy), n (creep exponent), V_a (activation volume) are experimentally determined flow law parameters and R is the gas constant.

Plasticity is implemented using the following yield criterion, which assumes fracture-related strain weakening (e.g.: Lavie et al., 2000; Huismans and Beaumont, 2002; Gerya, 2010a, 2013).

$$\sigma_{II} \leq C + \phi P$$

$$C = \begin{cases} C_a + (C_b - C_a) \times \frac{\gamma}{\gamma_{cr}}, & \text{if } \gamma \leq \gamma_{cr} \\ C_b, & \text{if } \gamma > \gamma_{cr} \end{cases}$$

$$\phi = \begin{cases} \phi_a + (\phi_b - \phi_a) \times \frac{\gamma}{\gamma_{cr}}, & \text{if } \gamma \leq \gamma_{cr} \\ \phi_b, & \text{if } \gamma > \gamma_{cr} \end{cases}$$

where σ_{II} is the second stress invariant, P is the dynamic pressure, γ is the integrated plastic strain and γ_{cr} is the upper strain limit for fracture related weakening. C and ϕ are the strength values (cohesion and friction angle) that depend on the plastic strain. C_a and ϕ_a are the initial and C_b and ϕ_b are final strength values, respectively. We assume that the plastic strength of fractured rocks is significantly lowered by percolating fluids and high pore fluid pressure.

The numerical formulation does not include elasticity. While elasticity may alter the short-term stress distribution in our models, the numerical formulation provides adequate first-order estimates on the long-term stress evolution of mountain belts that are assembled over millions of years (Kaus et al., 2008).

2.3. Surface processes

The topography of the model (air/crust interface) evolves according to a transport equation that is solved at each time-step on the Eulerian grid and accounts for erosion and sedimentation (e.g. Gorczyk and Vogt, 2015):

$$\frac{\partial z_{es}}{\partial t} = v_z - v_x \frac{\partial z_{es}}{\partial x} - v_s + v_e$$

where z_{es} is the vertical position of the surface as a function of the horizontal distance x ; v_z and v_x are the vertical and horizontal components of the material velocity vector at the surface; $v_s = 0.09 \text{ mm/yr}$ and $v_e = 0.9 \text{ mm/yr}$ are the sedimentation and erosion rates, respectively.

3. Results

Our results show that compression of two continental blocks, separated by a rheologically weak suture zone may result in (i) double-vergent orogens or (ii) continental subduction, with distinct geometries, deformation and exhumation patterns. The transition between these two different modes of collision is a direct consequence of the strength distribution within the continental lithosphere. Strong rheological coupling of upper and lower crust forms double vergent orogens, low rheological coupling results in continental subduction.

All varied parameters are summarized in Table 2.

3.1. Double-vergent orogens

Compression of the model domain initiates two oppositely dipping shear zones that are situated above the weak suture zone. In accordance with earlier studies, we call the left shear (i.e. foreland) pro-shear and the right shear (i.e. hinterland) retro shear, (Willett et al., 1993). The zone of deformation in pro-direction, i.e. the foreland (to the left in Fig. 2) is termed pro-wedge and the zone of deformation in retro-direction, i.e. the hinterland (to the right in Fig. 2) is called retro-wedge (Willett et al., 1993). First, the region between these shear zones is uplifted and forms a pop-up structure (Fig. 2). Subsequently, deformation localizes along the pro-shear (left thrust) and underlying weak zone, initiating large-scale asymmetry (Fig. 2). During early stages of convergence, movement along this shear zone accommodates most of the ongoing shortening. Later on, deformation propagates further to the left and forms a second pop-up, which is followed by successive thrusting (thrust napping) and fault-propagation (Fig. 2). This leads to distributed (i.e. diffuse) deformation on the pro-side and highly localized deformation on the retro-side (back thrust), which is in agreement with previous studies (e.g. Willett et al., 1993). Material transport along the highly localized retro-shear results in large offsets and lower crust exhumation (Fig. 2). At Moho depth, the progressive decoupling of crustal material from the mantle lithosphere, leads

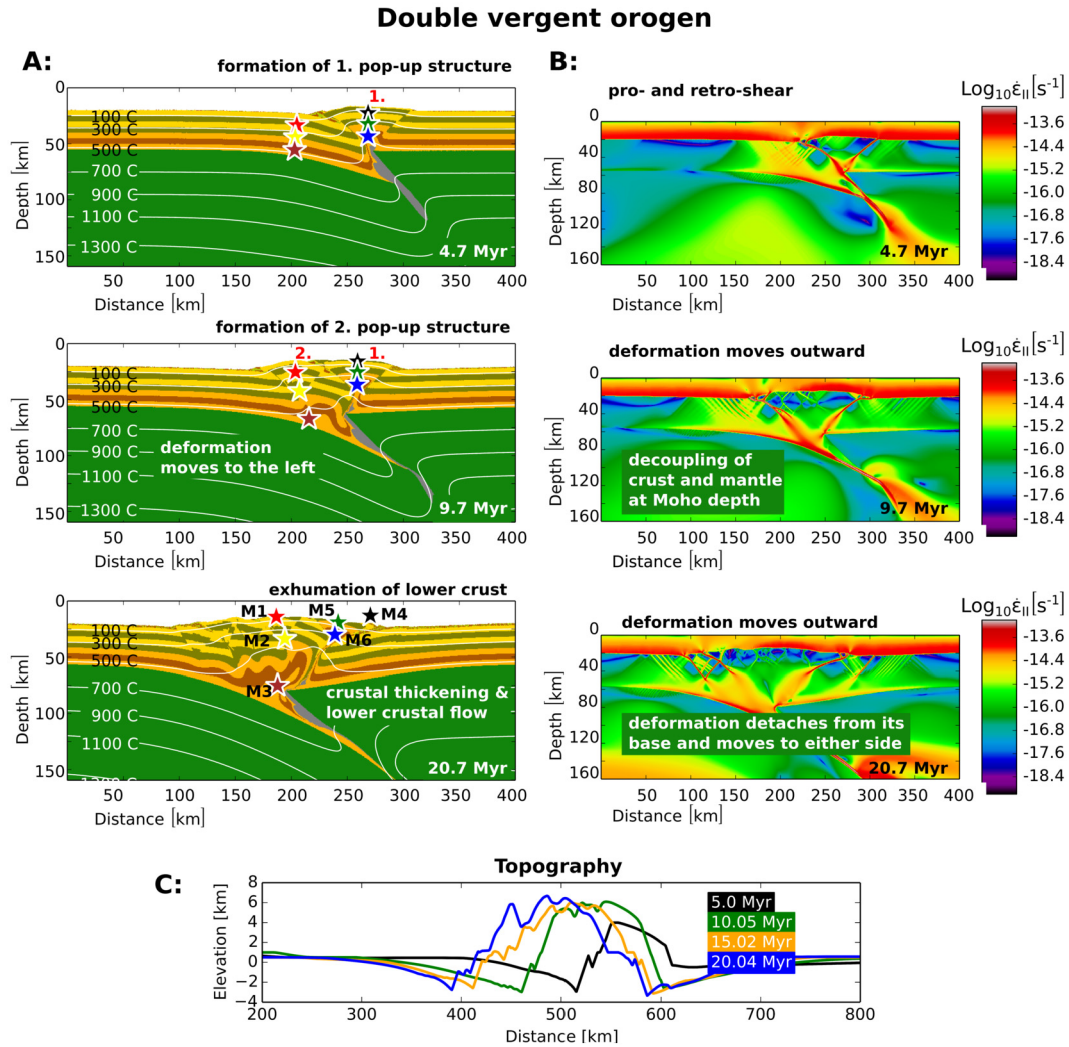


Fig. 2. Thermomechanical models showing the formation of a double vergent orogen (Exp. 1). The corresponding initial strength profile is shown in Fig. 1B1. **A** displays the compositional (lithological) field and rocks M1–M6 that have been traced through space and time. **B** shows the deformation pattern (second strain invariant). **C** shows the topographic evolution for time intervals of 5 Myr.

to subduction of mantle lithosphere and accumulation of lower crust material at the plate interface, against a backstop made of brittle upper mantle (Fig. 2). The continental crust is thickened and exhibits a thermally elevated inner core.

The resulting topography is overall symmetric with high elevations of up to 7 km in the centre of the domain and topographic depressions of up to 4 km on either side of the orogen (Fig. 2).

3.2. Continental subduction

Similar to double vergent orogens, the onset of convergence leads to an initially symmetric situation in which the pro- and retro-shear display limited offsets at the scale of the orogen. This is followed by localized deformation within the pro-shear and underlying weak zone, causing large-scale crustal asymmetry (Fig. 3). Subsequently, deformation moves beyond this shear to the left (pro-side), leaving the retro-side almost undeformed (Fig. 3). Low rheological coupling of upper and lower continental crust (Fig. 1B2) leads to strain partitioning and decoupling along the pro-side. The upper continental crust is subjected to intense shortening, whereas the lower continental crust remains coupled to the mantle lithosphere and subducts. The subducted lithosphere rolls back (towards the foreland) with respect to upper plate. The slab retreats and the sub-crustal structure forms a wedge-shaped

Moho. The resulting orogenic geometry is highly asymmetric and almost exclusively oriented towards the foreland (Fig. 3). Similar to double vergent orogens, highest offsets are recorded along the retro-shear (back-thrust), but, in contrast, are limited to exhumation depths of less than 10 km. The topographic response reflects the asymmetric geometry at depth with shallow surface slopes on the pro-side and somewhat higher slopes on the retro-side (Fig. 3).

3.3. Parametrical study

Ambient conditions may alter the stress distribution within the continental crust, and therefore, the resulting geometry of the mountain belt. To study this behaviour in more detail we have performed a series of additional experiments to verify the impact of the rate of collision, temperature and surface processes on the resulting geometry of the orogen.

Fig. 4 compares a coupled and a decoupled crust after the same amount of convergence, but different collision rates. At the onset of collision all experiments show a similar behaviour: After initial failure deformation localizes along the pro-shear and moves toward the incoming plate. In A (coupled crust), the successive nucleation and accretion of thrusts on the lower plate is accommodated by a highly localized back-thrust at the plate contact. The higher the convergence rate, the lower the offset at the back-

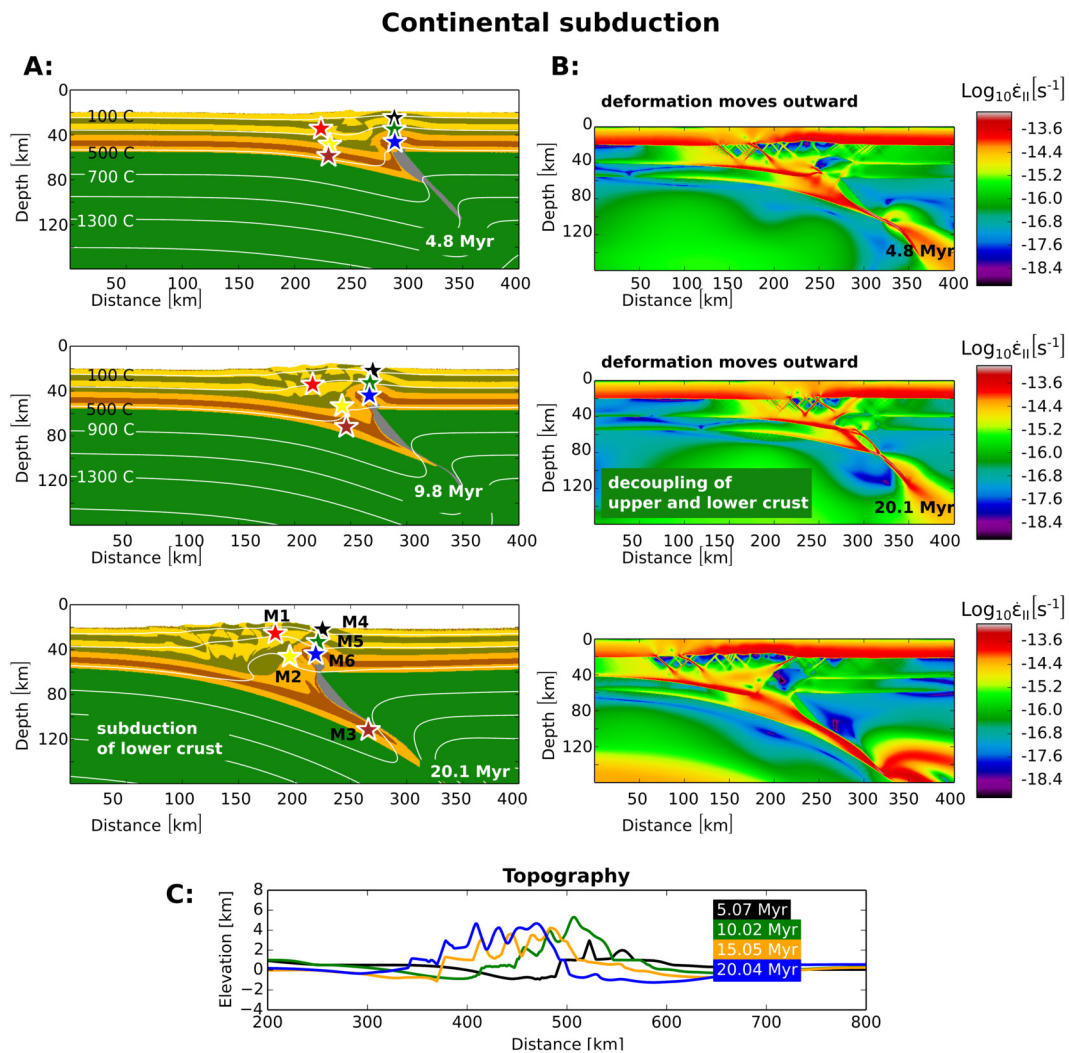


Fig. 3. Thermomechanical models showing continental subduction (Exp. 2). The corresponding initial strength profile is shown in Fig. 1B2. **A** displays the compositional (lithological) field and rocks M1–M6 that have been traced through space and time. **B** displays the deformation pattern (second strain invariant). **C** shows the topographic evolution for time intervals of 5 Myr.

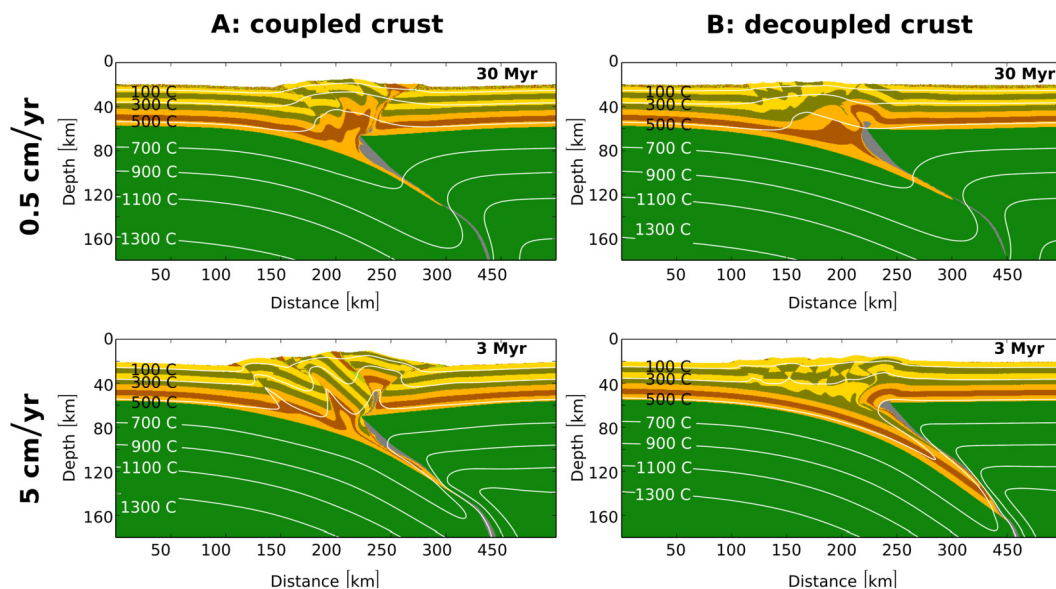


Fig. 4. Thermomechanical models showing the effect of strain rate (rate of compression) upon crustal accretion for **A**: coupled crust (Exp. 3, 4) and **B**: decoupled crust (Exp. 5, 6). High convergence in **A** increases the overall width of the orogen and the spacing of individual thrust units. It inhibits exhumation of lower crust in the back of the orogen. High convergence in **B** promotes subduction of lower continental crust. The resulting orogen is wider and no back-thrust is present.

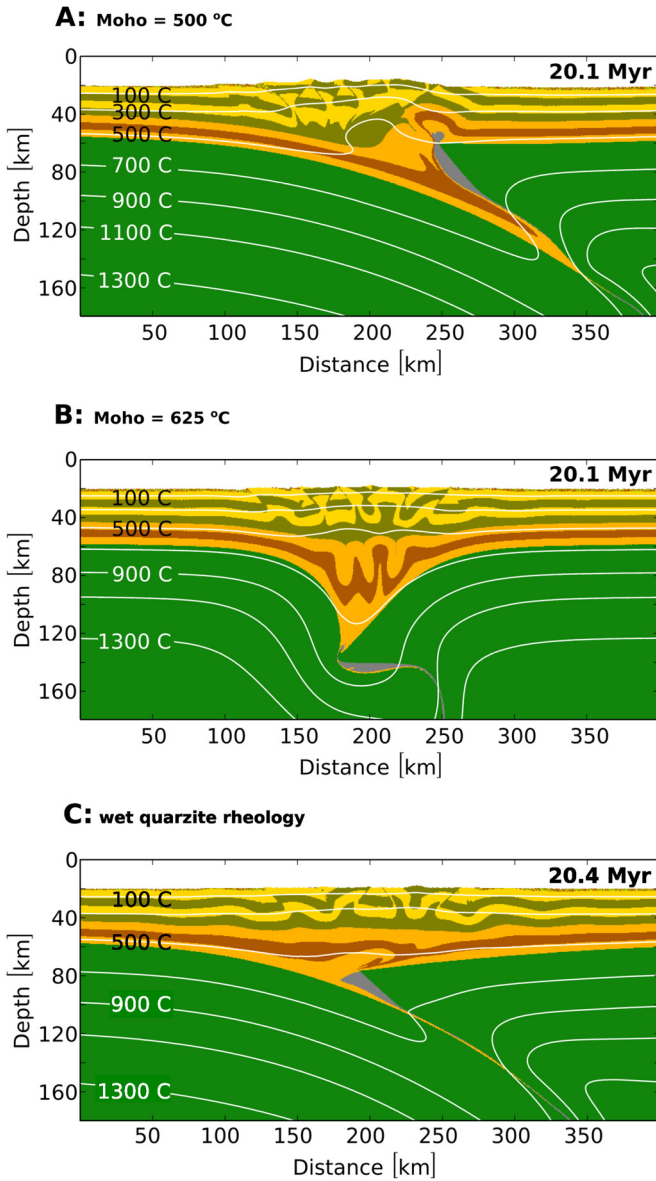


Fig. 5. Thermomechanical models demonstrating the effect of temperature and lower crust rheology on continental subduction (**A**: Exp. 2, **B**: Exp. 7, **C**: Exp. 8). Higher crustal strength in **A** results in continental subduction. Lower crustal strength in **B** and **C** leads to crustal thickening.

thrust and the greater the spacing of individual thrusts on the lower plate. In **B** (decoupled crust), the upper crust of the lower plate forms a sequence of foreland-propagating thrusts, while the lower crust is either accumulated against the brittle upper mantle (of the upper plate) or subducted. The higher the convergence, the greater the coupling of the lower crust and mantle, and therefore, the amount of continental subduction.

Fig. 5 shows the impact of a higher thermal gradient on continental subduction. In contrast to **A** (continental subduction as described above), deformation in **B** leads to crustal thickening rather than subduction. Viscous strength drops dramatically with increasing temperatures and the resulting orogen is symmetric, narrow and deeply rooted. Most of the crust flows and only the uppermost crust deforms in a brittle manner. Because the strength of the crust is also critically controlled by its rheology, we have conducted an additional experiment in which the entire continental crust is composed of wet quartzite rheology. Similar to **B**, convergence in **C** leads to crustal thickening and forms a sequence of

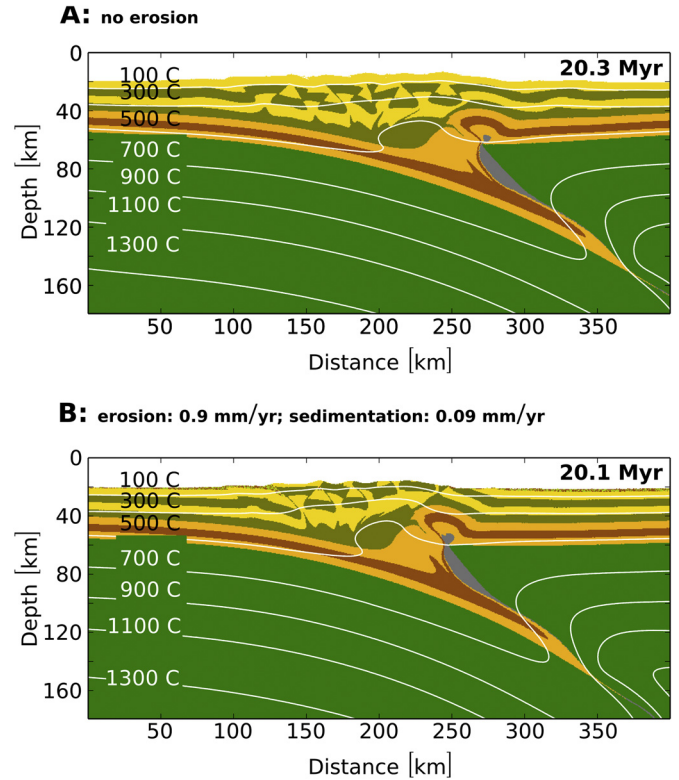


Fig. 6. **A** Thermomechanical model without erosion and sedimentation (Exp. 9) compared to **B**: our reference model of continental subduction, in which erosion and sedimentation are accounted for (Exp. 2). The overall geometry of **A** and **B** is very similar, despite differences in surface processes.

thrusts made of brittle upper crust. The lower crust resists subduction and spreads along the former suture zone. However, crustal thickening is less pronounced in **C** in comparison to **B**, because of its higher mantle strength.

Fig. 6 verifies the role of surface processes on continental collision. It shows that while differences in the local stress-field exist, the overall geometry of the orogen remains mostly unaffected by erosion and sedimentation. Only the width is greater in **A** (no erosion and no sedimentation) compared to **B** (erosion and sedimentation).

4. Discussion

4.1. Observations of natural examples of collision

Numerous examples are available for comparison between various collisional scenarios observed in nature. Double vergent orogens are high-convergence orogens with low angles of subduction. The contact between the collisional plates is often positioned in line with the location of slabs detected by teleseismic mantle tomography, such as in the European Alps ([Kissling et al., 2006](#)) (**Fig. 7a**). Crustal material is accreted to the upper plate along retro-shears, which are crustal-scale hinterland vergent backthrusts. Typical examples include the Pyrenees, the New Zealand Alps and the European Central Alps, where lower crustal rocks were exhumed along retro-shears during Oligocene–Miocene times ([Batt and Brandon, 2002](#); [Beaumont et al., 1996](#); [Schmid et al., 1996](#)).

In contrast, a number of low-topography mountain ranges at retreating subduction boundaries show continental subduction. In many of these cases the lower crust of the lower plate is decou-

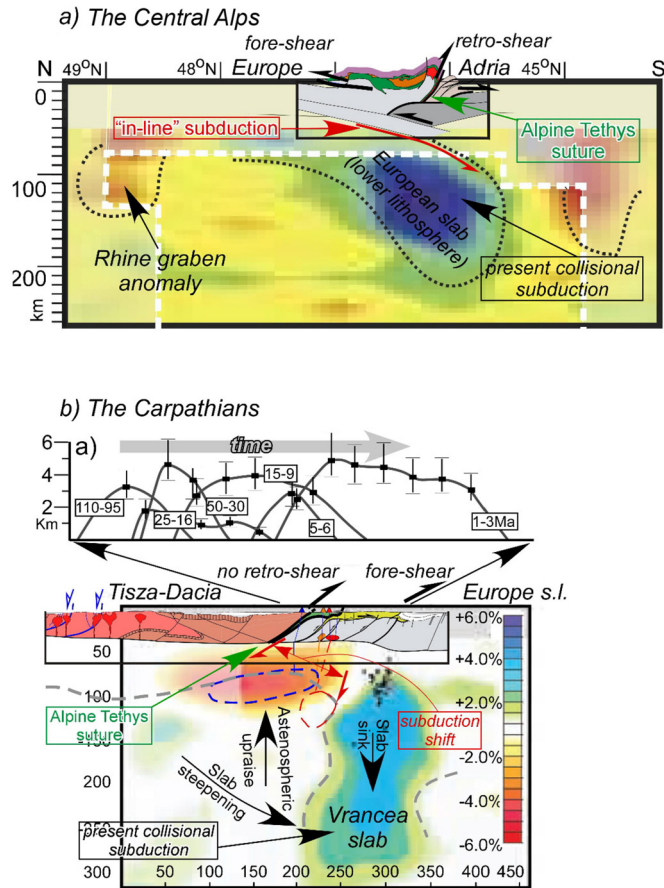


Fig. 7. A: double vergent orogen. Tectonic and teleseismic tomography cross-section of the European Central Alps modified after (Lippitsch et al., 2003; Schmid et al., 2004). The contact between the collisional plates is positioned in line with the slab. Exhumation is highest along the retro-shear. **B:** Continental subduction. Tectonic and teleseismic tomography cross-section of the SE Carpathians modified after (Martin et al., 2006; Matenco et al., 2010). The position of the slab is shifted to the foreland with respect to the former ocean–continent suture zone. The image above the transect shows exhumation values and ages derived from thermochronology (compiled and simplified from Merten, 2011). It demonstrates that exhumation has migrated towards the foreland during collision. See Matenco (2017) for further details.

pled and subducted into the mantle (Brun and Faccenna, 2008). The rapid roll-back of the slab is accommodated by upper plate extension and the formation of back-arc basins (Faccenna et al., 2004). This results in low amounts of shortening-related exhumation and the formation of highly arcuate thrust belts at the contact with the subduction zone (Jolivet and Faccenna, 2000; Merten et al., 2011). Examples of such collisional zones are concentrated in the Mediterranean: Carpathians, Dinarides, Apennines, Betics and Hellenides being examples of continental subduction (e.g. Faccenna et al., 2014; Matenco et al., 2010). In the Carpathians the contractional geometry was less affected by the backarc extension and is still preserved (Fig. 7b). It shows that the amount of collisional exhumation is restricted to 5–6 km and that deformation has migrated towards the foreland in time, because of the gradual deformation of the lower continental plate (Matenco, 2017) (Fig. 7b). Another common characteristic of continental subduction is the subduction shift, i.e. the position of slabs detected by teleseismic mantle tomography is shifted to the foreland and cannot be connected with the position of the former oceanic subduction suture zone (Fig. 7b). Such a shift contrasts with the typical “in-line” geometry of the retro-shear collision (Fig. 7a).

4.2. Mode of deformation

Numerous examples have proven that the rheology and strength distribution within the continental lithosphere have major implications on the structure of extensional and compressional systems (e.g. Beaumont and Quinlan, 1994; Brun, 2002; Willingshofer et al., 2013; Jammes and Huismans, 2012). The partitioning of plastic (brittle) and viscous (ductile) layering within the continental lithosphere was shown to control the mode of deformation: i.e. distributed versus localized deformation (e.g. Brun, 2002). For example, strain is localized when deformation of the brittle layer (competent layer) is compensated by the flow of ductile material, which enables perturbations in the upper brittle layer to amplify. The resulting orogen is narrow and records a highly localized strain pattern. If the viscosity of the ductile layer is too high to accommodate deformation of the brittle layer, deformation will propagate outward. The resulting orogen is wide and the strain pattern diffuses.

One of the main parameters controlling the viscous strength of rocks is temperature. Any change in the thermal gradient of the lithosphere will have profound implications on the mode of deformation. Additional experiments performed at higher thermal gradients (i.e.: Moho = 625 °C) demonstrate that the resulting orogen is narrow and deeply rooted, in contrast to their colder counterparts (Fig. 5). Because of the strength reduction with increasing temperature, all experiments result in continental thickening rather than subduction. This might have been a common scenario in the Precambrian when the ambient mantle temperatures and radiogenic heat production were higher (Sizova et al., 2014). Continental subduction, on the other hand, requires strength preservation (Figs. 3, 4). Our results are in agreement with previous studies, which have shown that subduction of continental lithosphere requires cold initial geotherms (Moho < 550 °C) and rapidly sinking plates (high convergence rates) to prevent thermal weakening due to heat diffusion (Burov and Yamato, 2008; Burov et al., 2014). A direct consequence of continental subduction are weakly developed retro-wedges (Fig. 3), which were shown to be a direct consequence of the rheological stratification of the continental lithosphere (Jammes and Huismans, 2012). Other parameters which can substantially influence the temperature field and, therefore, the rheological structure of an orogen are radioactive heating and viscous dissipation (Burg and Gerya, 2005; Faccenna et al., 2008).

Furthermore, lateral variations of rheological properties (Pfiffner et al., 2000) and structural inheritance from earlier tectonic phases may strongly modify the model evolution (Jammes and Huismans, 2012; Erdős et al., 2014).

4.3. Surface processes and material transport

4.3.1. Erosion and sedimentation

Special emphasis has been placed upon the effects of surface processes on the structural architecture of orogens. Because erosion and sedimentation result in the displacement of significant volumes of material, (changing the current stress distribution), important feedbacks between surface processes and tectonics are expected. Hence, several studies have focused on these feedbacks in the past (e.g. Willett et al., 1993; Willett, 1999; Burov, 2010; Erdős et al., 2014). It was concluded that sedimentation increases the length scale of thin- and thick-skinned thrust tectonics and results in wider orogens, while erosion favours localization, forming narrower orogens. Additional experiments performed in this study using a simple erosion/sedimentation approach demonstrate that varying the rate of erosion/sedimentation has a primary impact on the width of the orogen, but poses no substantial feedback on the structural architecture (geometry) (Fig. 6). Erosion reduces the

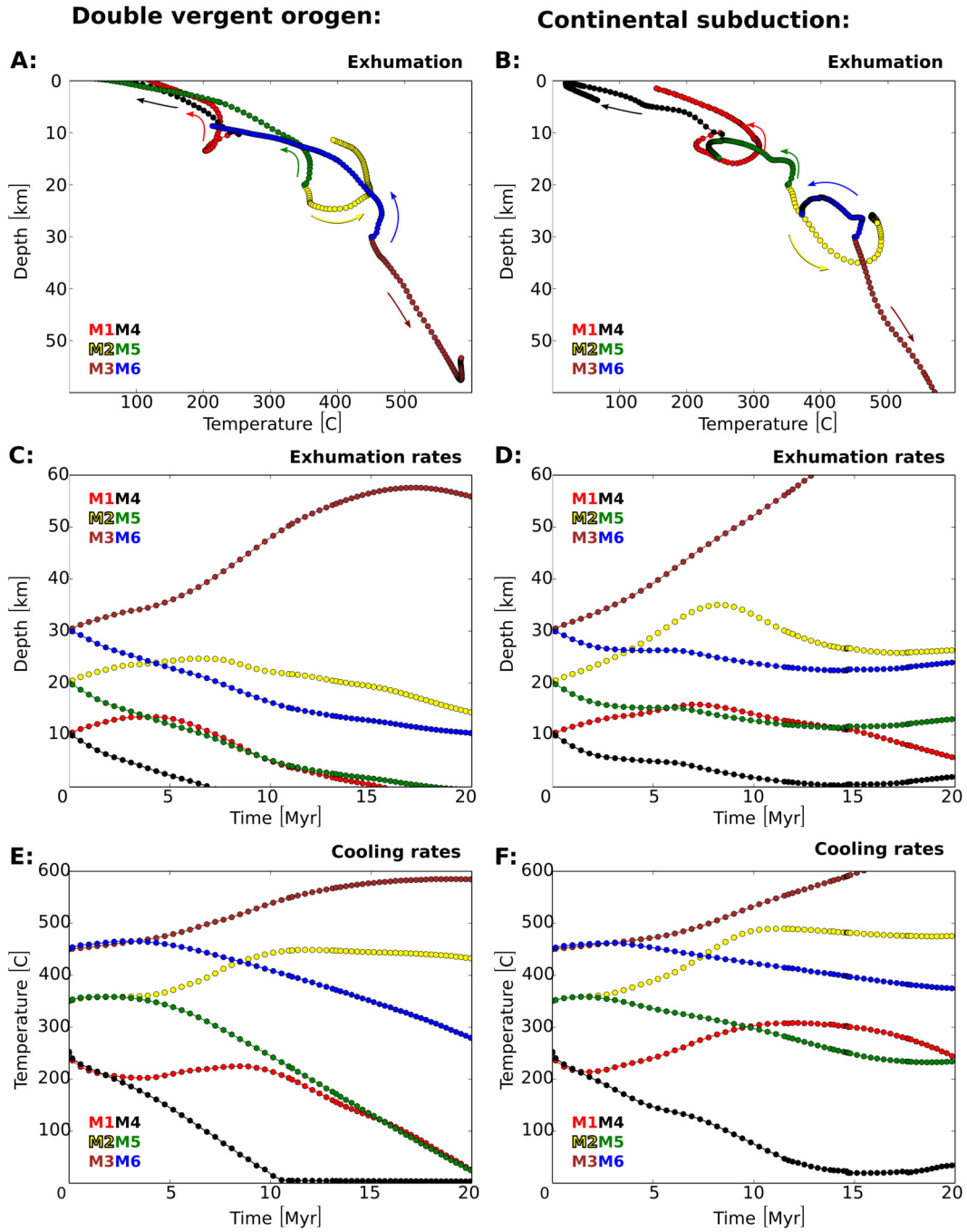


Fig. 8. Rock traces showing depth-temperature (exhumation **A, B**), depth-time (exhumation-rate **C, D**) and temperature-time (cooling rates **E, F**) relationships for double vergent orogens (left panel) and continental subduction (right panel). The corresponding rock tracers are shown in [Figs. 2 and 3](#).

thickness of the brittle upper crust and enables strain localization. This reduces the width of the orogen and enhances rock uplift/exhumation. However, asymmetric removal of surface material due to orographically controlled precipitation may alter not only the deformation pattern, but also the exhumation pattern ([Willett et al., 1993; Willett, 1999](#)).

4.3.2. Exhumation

In contrast, relatively little attention has been placed on the associated exhumation patterns and paths. We have, therefore, traced individual rocks located at 10 km, 20 km and 30 km depth forward in time ([Figs. 2, 3](#)). The resulting exhumation paths and rates are shown in [Fig. 8](#).

Highest offsets are recorded along retro-shears of double-vergent orogens ([Figs. 2 and 8A](#)). Intense and highly localized deformation allows for lower crust exhumation in contrast to continental subduction ([Fig. 8B](#)). Rocks initially located above the weak suture zone are transported along the retro shear towards the surface at rates of about 1 mm/yr (M4) to 1.5 mm/yr (M5) ([Fig. 8C](#)). Similar rates of around 1 mm/yr (M1) can be obtained from upper crustal rocks (<10 km) initially located on the pro-side. In comparison, decoupling of upper and lower crust material during continental subduction allows for subduction of lower continental crust and results in limited offsets (<10 km) and somewhat slower rates of 0.5 mm/yr (M4) ([Fig. 8D](#)). The corresponding cooling rates are shown in [Fig. 8E and 8F](#).

These rates are in general agreement with late stage exhumation speeds of collisional systems reported by Vogt and Gerya (2014). Nevertheless, one should keep in mind that oceanic subduction preceding continental collision might have profound implications on crustal burial and exhumation (Burov and Yamato, 2008; Burov et al., 2014; Vogt and Gerya, 2014).

5. Conclusions

Deformation in continent–continent collision zones may result in double vergent orogens or continental subduction, depending on the rheological structure of the continental lithosphere. Strong rheological coupling of upper and lower continental crust results in the formation of a décollement at Moho depth that separates the downgoing mantle lithosphere from the accreting continental crust. The resulting geometry is double vergent. In contrast, low rheological coupling of upper and lower continental crust forms a décollement at mid-crustal levels. Only the upper continental crust is accreted frontally; the lower crust sinks into the mantle, resulting in continental subduction.

These results suggest that double-vergent orogens such as the Central European Alps formed at high convergence plate boundaries where the crustal coupling, temperature distribution and rate of deformation allow the transport of lower crustal material in retro-wedges at high rates of exhumation. In contrast, retreating collisional orogens such as the Carpathians record crustal decoupling in similar conditions of temperature and strain rates, resulting in continental subduction of lower crust, migration of plate boundaries towards the foreland and lower amounts of hinterland exhumation.

Acknowledgements

This study has been supported by the Netherlands Research Centre for Integrated Solid Earth Sciences (ISES). We thank Taras Gerya for providing the numerical code i2vis and for comments on an earlier version of this manuscript. In depth reviews by Alexander Koptev and an anonymous reviewer helped improving the quality of the manuscript. All simulations were run on the Brutus cluster at ETH Zurich.

References

- Batt, G.E., Brandon, M.T., 2002. Lateral thinking: 2-D interpretation of thermochronology in convergent orogenic settings. *Tectonophysics* 349 (1), 185–201.
- Beaumont, C., Ellis, S., Hamilton, J., Fullsack, P., 1996. Mechanical model for subduction–collision tectonics of Alpine-type compressional orogens. *Geology* 24 (8), 675–678.
- Beaumont, C., Quinlan, G., 1994. A geodynamic framework for interpreting crustal-scale seismic-reflectivity patterns in compressional orogens. *Geophys. J. Int.* 116 (3), 754–783.
- Brun, J.-P., 2002. Deformation of the continental lithosphere: insights from brittle–ductile models. *Geol. Soc. (Lond.) Spec. Publ.* 200 (1), 355–370.
- Brun, J.-P., Faccenna, C., 2008. Exhumation of high-pressure rocks driven by slab rollback. *Earth Planet. Sci. Lett.* 272 (1–2), 1–7.
- Burg, J.-P., Gerya, T., 2005. The role of viscous heating in Barrovian metamorphism of collisional orogens: thermomechanical models and application to the Lepontine Dome in the Central Alps. *J. Metamorph. Geol.* 23 (2), 75–95.
- Burov, E., 2010. Thermo-mechanical models for coupled lithosphere–surface processes: applications to continental convergence and mountain building processes. In: Cloetingh, S.A.P.L., Negendank, J. (Eds.), *New Frontiers in Integrated Solid Earth Sciences*. Springer, pp. 103–143.
- Burov, E., François, T., Agard, P., Le Pourhiet, L., Meyer, B., Tirel, C., Lebedev, S., Yamato, P., Brun, J.-P., 2014. Rheological and geodynamic controls on the mechanisms of subduction and HP/UHP exhumation of crustal rocks during continental collision: insights from numerical models. *Tectonophysics* 631, 212–250.
- Burov, E., Yamato, P., 2008. Continental plate collision, P–T–t conditions and unstable vs. stable plate dynamics: insights from thermo-mechanical modelling. *Lithos* 103 (1–2), 178–204.
- Carminati, E., Doglioni, C., 2012. Alps vs. Apennines: the paradigm of a tectonically asymmetric Earth. *Earth-Sci. Rev.* 112 (1–2), 67–96.
- Davis, D., Suppe, J., Dahlen, F., 1983. Mechanics of fold-and-thrust belts and accretionary wedges. *J. Geophys. Res.* 88 (B2), 1153–1172.
- Ellis, S., Wissing, S., Pfiffner, A., 2001. Strain localization as a key to reconciling experimentally derived flow-law data with dynamic models of continental collision. *Int. J. Earth Sci.* 90 (1), 168–180.
- Erdős, Z., Huismans, R.S., van der Beek, P., Thieulot, C., 2014. Extensional inheritance and surface processes as controlling factors of mountain belt structure. *J. Geophys. Res., Solid Earth* 119 (12), 9042–9061.
- Faccenna, M., Gerya, T.V., Chakraborty, S., 2008. Styles of post-subduction collisional orogeny: influence of convergence velocity, crustal rheology and radiogenic heat production. *Lithos* 103 (1–2), 257–287.
- Faccenna, C., Becker, T.W., Auer, L., Billi, A., Boschi, L., Brun, J.P., Capitanio, F.A., Fucciello, F., Horváth, F., Jolivet, L., et al., 2014. Mantle dynamics in the Mediterranean. *Rev. Geophys.* 52 (3), 283–332.
- Faccenna, C., Piromallo, C., Crespo-Blanc, A., Jolivet, L., Rossetti, F., 2004. Lateral slab deformation and the origin of the western Mediterranean arcs. *Tectonics* 23 (1).
- Forte, A.M., Cowgill, E., Whipple, K.X., 2014. Transition from a singly vergent to doubly vergent wedge in a young orogen: the Greater Caucasus. *Tectonics* 33 (11), 2077–2101.
- Gerya, T., 2010a. Dynamical instability produces transform faults at mid-ocean ridges. *Science* 329 (5995), 1047–1050.
- Gerya, T., 2010b. *Introduction to Numerical Geodynamic Modelling*. Cambridge University Press.
- Gerya, T., Yuen, D., 2003. Characteristics-based marker-in-cell method with conservative finite-differences schemes for modeling geological flows with strongly variable transport properties. *Phys. Earth Planet. Inter.* 140 (4), 293–318.
- Gerya, T.V., 2013. Three-dimensional thermomechanical modeling of oceanic spreading initiation and evolution. *Phys. Earth Planet. Inter.* 214, 35–52.
- Gorczyk, W., Vogt, K., 2015. Tectonics and melting in intra-continental settings. *Gondwana Res.* 27 (1), 196–208.
- Huismans, R.S., Beaumont, C., 2002. Asymmetric lithospheric extension: the role of frictional plastic strain softening inferred from numerical experiments. *Geology* 30 (3), 211–214.
- Jammes, S., Huismans, R.S., 2012. Structural styles of mountain building: controls of lithospheric rheologic stratification and extensional inheritance. *J. Geophys. Res., Solid Earth* 117, B10.
- Jolivet, L., Faccenna, C., 2000. Mediterranean extension and the Africa–Eurasia collision. *Tectonics* 19 (6), 1095–1106.
- Kaus, B.J., Steedman, C., Becker, T.W., 2008. From passive continental margin to mountain belt: insights from analytical and numerical models and application to Taiwan. *Phys. Earth Planet. Inter.* 171 (1), 235–251.
- Kissling, E., Schmid, S.M., Lippitsch, R., Ansorge, J., Fügenschuh, B., 2006. Lithosphere structure and tectonic evolution of the Alpine arc: new evidence from high-resolution teleseismic tomography. *Mem. Geol. Soc. Lond.* 32 (1), 129–145.
- Lavier, L.L., Buck, W.R., Poliakov, A.N.B., 2000. Factors controlling normal fault offset in an ideal brittle layer. *J. Geophys. Res., Solid Earth* 105 (B10), 23431–23442.
- Lippitsch, R., Kissling, E., Ansorge, J., 2003. Upper mantle structure beneath the Alpine orogen from high-resolution teleseismic tomography. *J. Geophys. Res., Solid Earth* 108 (B8).
- Malavieille, J., 1984. Modelisation experimentale des chevauchements imbriques; application aux chaines de montagnes. *Bull. Soc. Géol. Fr. S7-XXVI* (1), 129–138.
- Martin, M., Wenzel, F., CALIXTO Working Group, 2006. High-resolution teleseismic body wave tomography beneath SE-Romania-II. Imaging of a slab detachment scenario. *Geophys. J. Int.* 164 (3), 579–595.
- Matenco, L., 2017. Tectonics and exhumation of the Romanian Carpathians: inferences from kinematic and thermochronological studies. In: Radoane, M., Vespereanu-Stroe, A. (Eds.), *Landform Dynamics and Evolution in Romania*, pp. 15–56.
- Matenco, L., Krézsek, C., Merten, S., Schmid, S., Cloetingh, S., Andriessen, P., 2010. Characteristics of collisional orogens with low topographic build-up: an example from the Carpathians. *Terra Nova* 22 (3), 155–165.
- Merten, S., 2011. *Thermo-Tectonic Evolution of a Convergent Orogen with Low Topographic Build-Up: Exhumation and Kinematic Patterns in the Romanian Carpathians Derived from Thermochronology*. Ph.D. thesis. Vrije Universiteit Amsterdam.
- Merten, S., Matenco, L., Foeken, J., Andriessen, P., 2011. Toward understanding the post-collisional evolution of an orogen influenced by convergence at adjacent plate margins: Late Cretaceous–Tertiary thermotectonic history of the Apuseni Mountains. *Tectonics* 30 (6).
- Morley, C., 2012. Late Cretaceous–Early Palaeogene tectonic development of SE Asia. *Earth-Sci. Rev.* 115 (1–2), 37–75.
- Pfiffner, O., Ellis, S., Beaumont, C., 2000. Collision tectonics in the Swiss Alps: insight from geodynamic modeling. *Tectonics* 19 (6), 1065–1094.
- Ranalli, G., 1995. *Rheology of the Earth*. Springer, p. 334.
- Schmid, S.M., Fügenschuh, B., Kissling, E., Schuster, R., 2004. Tectonic map and overall architecture of the Alpine orogen. *Eclogae Geol. Helv.* 97 (1), 93–117.
- Schmid, S.M., Pfiffner, O., Froitzheim, N., Schönborn, G., Kissling, E., 1996. Geophysical–geological transect and tectonic evolution of the Swiss–Italian Alps. *Tectonics* 15 (5), 1036–1064.

- Sizova, E., Gerya, T., Brown, M., 2014. Contrasting styles of Phanerozoic and Precambrian continental collision. *Gondwana Res.* 25 (2), 522–545.
- Turcotte, D., Schubert, G., 2002. *Geodynamics*. Cambridge University Press.
- Vogt, K., Gerya, T.V., 2014. From oceanic plateaus to allochthonous terranes: numerical modelling. *Gondwana Res.* 25 (2), 494–508.
- Willett, S., Beaumont, C., Fullsack, P., 1993. Mechanical model for the tectonics of doubly vergent compressional orogens. *Geology* 21 (4), 371–374.
- Willett, S.D., 1999. Orogeny and orography: the effects of erosion on the structure of mountain belts. *J. Geophys. Res., Solid Earth* 104 (B12), 28957–28981.
- Willingshofer, E., Sokoutis, D., Luth, S., Beekman, F., Cloetingh, S., 2013. Subduction and deformation of the continental lithosphere in response to plate and crust–mantle coupling. *Geology* 41 (12), 1239–1242.